Three-dimensional modeling and reconstructive change of residual stress during machining process of milling, polishing, heat treatment, vibratory finishing, and shot peening of fan blade

Ji-Yin Zhang[1,2] · Chang-Feng Yao[1,2] · Min-Chao Cui[1,2] · Liang Tan[1,2] ·
Yun-Qi Sun[1,2]

Abstract Residual stress during the machining process has always been a research hotspot, especially for aero-engine blades. The three-dimensional modeling and reconstructive laws of residual stress among various processes in the machining process of the fan blade is studied in this paper. The fan blades of Ti-6Al-4V are targeted for milling, polishing, heat treatment, vibratory finishing, and shot peening. The surface and subsurface residual stress after each process is measured by the X-ray diffraction method. The distribution of the surface and subsurface residual stress is analyzed. The Rational Taylor surface function and cosine decay function are used to fit the characteristic function of the residual stress distribution, and the empirical formula with high fitting accuracy is obtained. The value and distribution of surface and subsurface residual stress vary greatly due to different processing techniques. The reconstructive change of the surface and subsurface residual stress of the blade in each process intuitively shows the change of the residual stress between the processes, which has a high reference significance for the research on the residual stress of the blade processing and the optimization of the entire blade process.

✉ Chang-Feng Yao
chfyao@nwpu.edu.cn

1 Key Laboratory of High Performance Manufacturing for Aero Engine, Northwestern Polytechnical University, Ministry of Industry and Information Technology, Xi'an 710072, People's Republic of China

2 Engineering Research Center of Advanced Manufacturing Technology for Aero Engine, Northwestern Polytechnical University, Ministry of Education, Xi'an 710072, People's Republic of China

1 Introduction

Residual stress is the stress that exists in an object in equilibrium when there is no stress. In the manufacturing process of parts, residual stress will be generated inside the parts. When parts are machined, it is rare that no residual stress is generated inside the component. The state of residual stress introduced by processing, especially the magnitude of its stress value, varies with the processing method or treatment method. Residual stress is generated in various machining processes of the workpiece, such as milling, polishing, heat treatment, vibratory finishing, shot peening, and so on. Residual stress has a great influence on the application of workpieces, especially thin-walled parts [1, 2]. Many scholars have done a lot of research on the residual stress in each processing process.

There are many kinds of blades, and their respective processing processes also differ. The main processes for fan blades are milling, polishing, heat treatment, vibratory finishing and shot peening. Milling is the process of removing excess material according to the design model. The milling process introduces residual stresses due to tearing and extrusion of the material. Milling parameters play a large role in the residual stress, and the residual stress has a significant impact on the quality of the milling process. The influences of milling parameters like cutting speed, feed rate, and depth of cut on the residual stress distribution have been studied [3–6]. For the prediction of residual stress after milling, the response surface method was used [7] and the models for predicting the surface and

subsurface residual stress distributions of milling via process conditions were developed [8–11]. The polishing process mainly reduces the roughness, and at the same time reduces the compressive residual stress and makes its distribution more uniform. Based on the traditional polishing process, some new types of polishing process are increasingly used in the polishing process, such as hydrodynamic suspension polishing [12], and flexible polishing [13, 14]. Especially, the belt polishing, bob polishing, and flexible polishing are commonly used in the precision manufacturing of gas turbine engine components for aerospace and energy applications [15]. There are also studies on the effects of different types of polishing processes on the residual stress distribution [16, 17]. Heat treatment usually used to release the residual stress after the previous process [18–21]. A novel cryogenic treatment is used to reduce the residual stress and improve the mechanical property [22]. The effect of the post weld heat treatment on the residual stress has been studied by the Norton creep law model [23]. The change of residual stress during the annealing process has been predicted by a novel residual stress relaxation model [24]. Research on vibratory finishing mainly focuses on the surface roughness [25] and residual stress [26]. The vibratory finishing is extensively utilized in the manufacturing process of aircraft engine blades [27, 28]. The residual stress of the part can be reduced by a part, and it can also become uniform. The normal force, material removal and surface topography of vibratory finishing were analyzed and correlated to understand the cause-effect relationships, and then enable the efficient surface smoothing and improved residual stress depth distribution [29]. Shot peening improves the fatigue resistance of specimens by introducing high compressive residual stress. The research of residual stress distribution after shot peening mostly adopts finite element analysis [30, 31] and experiment [32], and the residual stress value and the uniformity of the residual stress distribution are both research goals [33]. The model to predict the residual stress distribution induced by shot peening has also been presented [34]. Other shot peening methods such as water jet peening give a surface layer residual stress equivalent better than that of normal shot peening [35]. The effects of shot peening time on the residual stress evolution in the process of shot peening have been investigated [36]. There are also a lot of researches on the distribution of residual stress after the composite machining process [37–40].

At present, most of the research focuses on the residual stress of a single machining process, and there are few studies on the change of residual stress between multiple processes. The fan blade was used as the research object in this paper; the milling, polishing, heat treatment, vibratory finishing, and shot peening processes were performed; and the residual stresses were measured. The surface and subsurface residual stresses of each process are analyzed, and the reconstructive change of the residual stress between processes is studied by fitting empirical formulas. It has important reference significance for studying the residual stress in the whole process of fan blade.

2 Machining of fan blade and measuring of residual stress

A large fan blade of aeroengine is studied in this paper, and the material of the fan blade is Ti-6Al-4V. The fan blade has a more complex geometry with three-dimensional freeform surface, therefore, the complicated processing technology is needed. The machining process of the fan blade from blank to finished product is shown in Fig. 1. The blade was milled on the DMU125P five-axis machining center of Gildemeister, and it was polished with the 2MY55200-6NC belt polishing machine of Chongqing Samhida Grinding Machine Co. Ltd. The heat treatment was carried out in the HVA-8812S vacuum heat treatment furnace of ACME; the vibratory finishing process was then completed on Rotary Vibrator R 420 DL of Rosler; and finally, the shot peening process was done on MP1500TX shot peening equipment of Wheelabrator.

After the blade was processed by various processes, the residual stress was measured. The measurement points were carefully chosen to ensure that the measured residual stress reflected the residual stress distribution in the blade as closely as possible. On the surface of the blade, 20 measurement points were distributed as evenly as possible to measure surface residual stress. To measure the subsurface residual stress, 18 measurement points were distributed as evenly as possible as shown in Fig. 2. As the heat treatment and vibratory finishing in the blade process do not have a clear machining direction, only the residual stress in the x-direction is measured, as shown in Fig. 2.

The PROTO-LXRD MG2000 residual stress measurement system is used to measure the surface and subsurface residual stresses of the thin-walled fan blade. Residual stress measurement is realized based on the X-ray diffraction technique. The basic principle is that the lattice strain and the macroscopic strain of a material caused by a certain stress are the same, and the lattice strain can be measured by the X-ray diffraction technique and the macroscopic strain can be obtained from elastic mechanics. The macroscopic stress can be deduced from the measured lattice strain. In the process of residual stress measurement, the $\sin^2 \psi$ method of X-ray diffraction stress analysis is used. According to the Bragg equation, the stress calculation equation can be obtained as
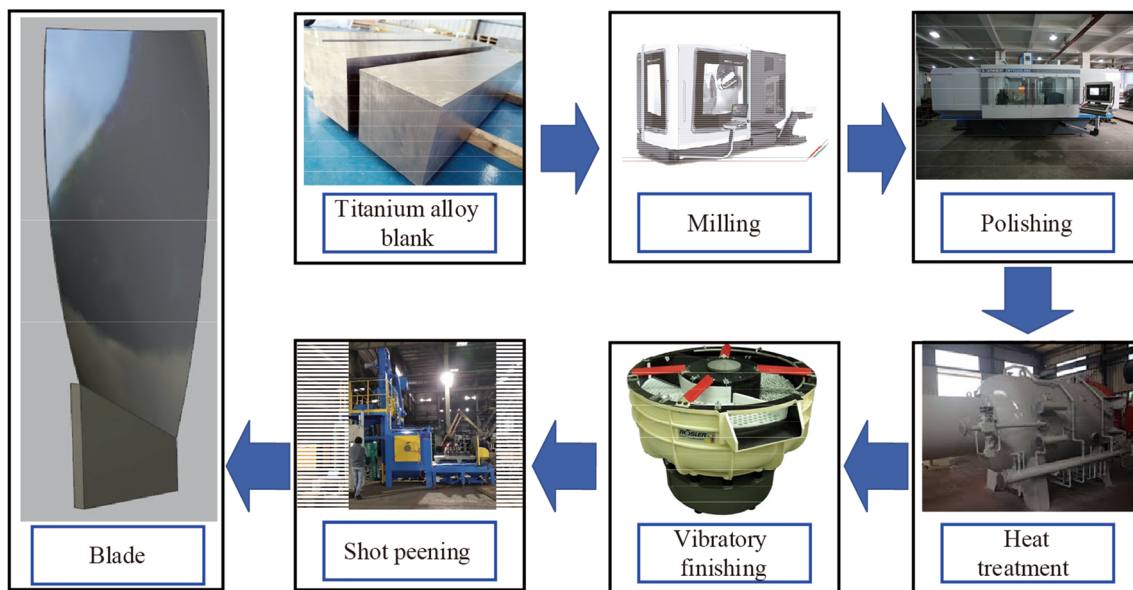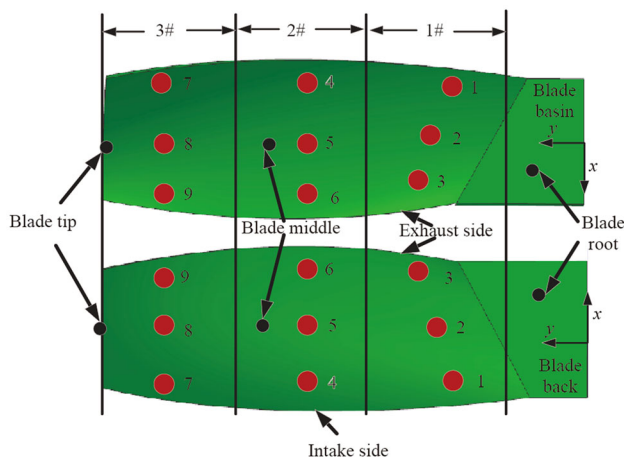
Fig. 1 Machining process of fan blade

Fig. 2 Fan blade

$$\sigma = KM, \tag{1}$$

$$K = -\frac{1}{2}\cot\theta_0\left(\frac{\pi}{180}\right)\left(\frac{E}{1+v}\right)_{hkl}, \tag{2}$$

$$M = \frac{\partial 2\theta_{\phi,w}}{\partial \sin^2\psi}, \tag{3}$$

where σ is the residual stress; K is the X-ray stress constant, MPa/(°); θ_0 is the diffraction angle in the stress-free state; $2\theta_{\phi,w}$ is the X-ray diffraction angle; ψ is the angle between the normal of the diffraction crystal plane (*hkl*) and the normal of the material surface; M is the slope of the diffraction angle position corresponding to different ψ

directions $2\theta_{\phi,w}$ and $\sin^2\psi$ linear relationship. The key to the residual stress measurement is to accurately determine the diffraction angle $2\theta_{\phi,w}$, and then find the value of residual stress according to the stress calculation equation.

To obtain the distribution of residual stress along the depth, the blade surface was electropolished with a saturated solution of $CH_3OH:C_6H_{14}O_2:HClO_4 = 10:5:1$ to expose the deeper layers. Firstly, the surface residual stress and the original thickness perpendicular to the measurement point were measurement. The electrolytic polishing equipment is then used to corrode the local area, and the depth of corrosion is controlled by adjusting the electrolysis time and number of times. Then the residual stress in the *x*-direction of each layer is measured until multiple residual stress values are close to a certain stress value. It can be considered that the measured residual stress value is the same as the residual stress of the material matrix. When measuring the subsurface residual stress after corrosion, the corrosion area is a circle with a diameter of 5mm, which is smaller than the blade profile (600 mm × 150 mm). The deformation caused by the corrosion removal has little impact on the residual stress and can be ignored. At the same time, the diameter and depth of the corrosion area are input into the measurement system, and the residual stress measurement system will automatically compensate, further ensuring the accuracy of the residual stress measure.

Considering various factors, the parameters for measuring the residual stress of Ti-6Al-4V are shown in Table 1.

Table 1 Parameter for measuring the residual stress of Ti-6Al-4V

Voltage/ kV	Electric current/mA	X-ray transistor	β angle/ (°)	Exposure number	Exposure time/s	Bragg angle 2θ/(°)	Diffraction crystal plane	Collimator diameter/mm
25	20	CuK_α	± 25	10	2	142	{213}	3

Before measuring the residual stress, the equipment has been debugged by experienced testers for many times, and the error of the measurement result can be kept within ± 30 MPa. The results are very accurate, and the error can be ignored during the analysis.

3 Analysis of surface residual stress of the blade

3.1 Distribution of surface residual stress of the blade

After the residual stresses of the blade are measured, the surface residual stresses of the measured points on each blade are analyzed and the residual stress distribution based on the blade surface coordinates can be obtained by function fitting. The distributions of the surface residual stress of the blade after milling, polishing, heat treatment, vibratory finishing, and shot peening are described in Fig. 3 with the contour map of residual stress. In the figure, the x-axis and the y-axis respectively represent the x coordinate axis and the y coordinate axis of the blade design coordinate system, and the magnitude of the residual stress value is indicated by color. The dark blue area indicates that the compressive residual stress is large; the dark red area indicates that the compressive residual stress is small; and the transition from dark blue to dark red color also represents the decrease of the compressive residual stress value.

As can be seen from Fig. 3, the surface residual stress profile and its value in the blade back and the blade basin are very different, depending on the blade structure and the different processing techniques. And the maximum and minimum compressive residual stresses in the surface of the blade back and the blade basin are different due to different processing techniques. After the blade is milled, the maximum surface residual stress in the blade back is located in the ridge area of blade root, with a value of −405.30 MPa. The minimum surface residual stress is located in the exhaust side area of blade middle, with a value of −250.39 MPa. In addition, the maximum surface residual stress in the blade basin is located at the exhaust side area of blade root with a value of −380.56 MPa, and the minimum surface residual stress is located at the intake side area of blade middle with a value of −210.56 MPa.

The extreme values of the compressive residual stress of milling, polishing, heat treatment, vibratory finishing, and shot peening are shown in Tables 2 and 3. Based on the milling process parameters and blade structure, the surface residual stress caused by the milling process is from −200 MPa to −400 MPa, and its surface residual stress range is from −100 MPa to −350 MPa after polishing. Then the heat treatment is carried out to eliminate the residual stress, its surface residual stress range becomes from 20 MPa to −90 MPa. Because of the vibration finishing treatment, its surface compressive residual stress increases to the range between −300 MPa and −530 MPa, and finally the shot peening further improve its compressive residual compressive stress to the range between −650 MPa and −800 MPa.

Comprehensive analysis found that the residual stresses in the surface of the blade back and blade basin are all compressive residual stresses, and there is no consistent law of distribution.

3.2 Statistics of residual stress on the blade surface

The measured value of the surface residual stress of each process is statistically analyzed, and the approximate range of the residual stress value of each process is evaluated. The statistical content of residual stress is shown in Fig. 4. The axis of abscissa represents the interval of residual stress values, and the axis of ordinate represents the number of values in each interval of residual stress. And the specific number in the interval of each residual stress value is indicated on the histogram.

It can be seen from Fig. 4 that the surface residual stress value of the blade after milling is mainly concentrated between −240 MPa and −360 MPa; the residual stress value of polishing is mainly concentrated between −200 MPa and −300 MPa; and the residual stress value of heat treatment is mainly concentrated between −20 MPa and −80 MPa; the residual stress value of vibratory finishing mainly concentrated between −360 MPa and −440 MPa; the residual stress value of shot peening mainly concentrated between −660 MPa and −720 MPa. Comprehensively comparing the distribution range of the residual stress value on the blade surface of each process, it is found that the distribution range of the residual stress
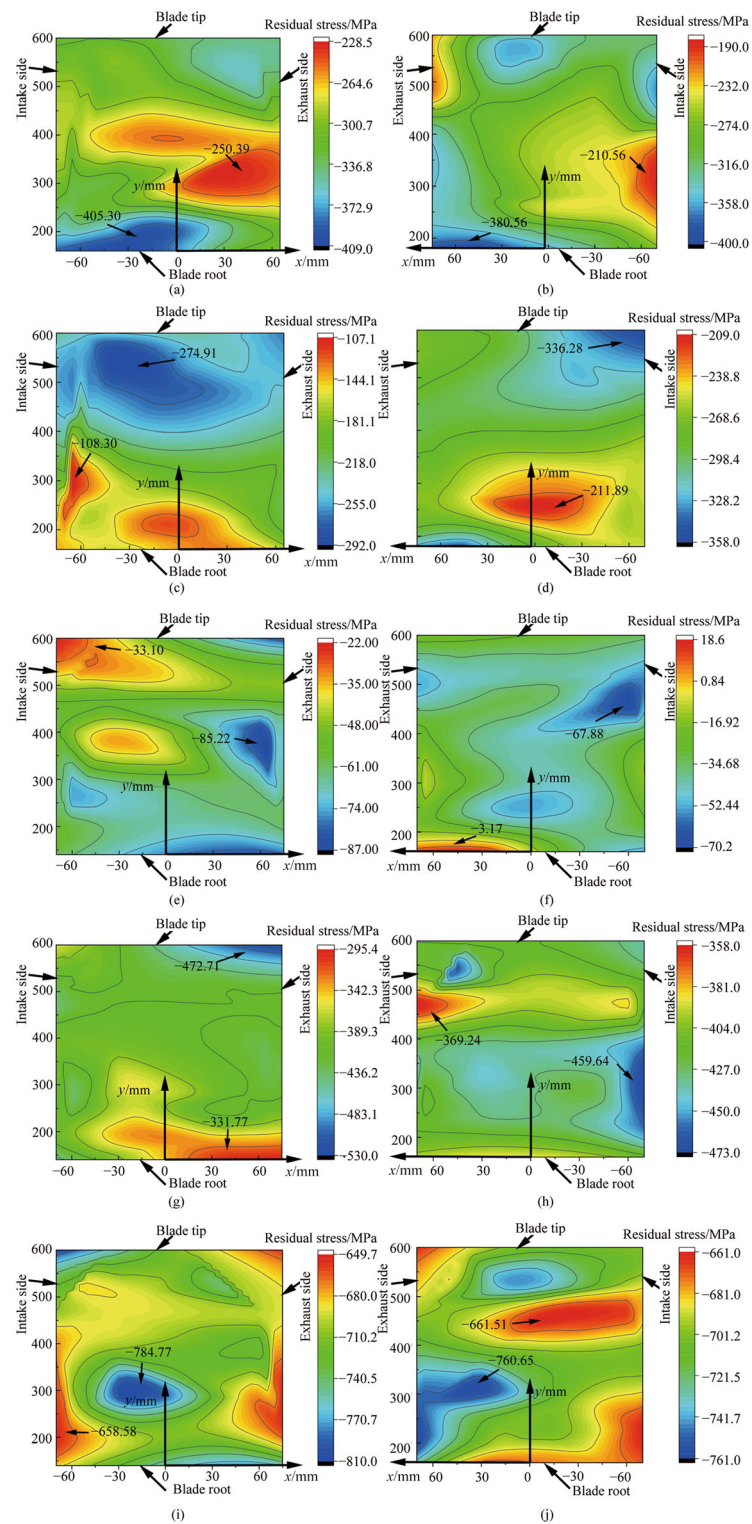
Fig. 3 Distributions of surface residual stress in the blade **a** blade back of milled blade, **b** blade basin of the milled blade, **c** blade back of the blade after polishing, **d** blade basin of the blade after polishing, **e** blade back of the blade after heat treatment, **f** blade basin of the blade after heat treatment, **g** blade back of blade after vibratory finishing, **h** blade basin of the blade after vibratory finishing, **i** blade back of blade after shot peening, **j** blade basin of the blade after shot peening

value of the blade after milling and polishing is large; the residual stress difference is relatively large; and it is easy to cause large processing deformation, so the processing process needs to be further optimized. The distribution range of the residual stress values of the blades after heat treatment, vibratory lighting and shot peening is small, which indicates that they have a high processing consistency. However, the heat treatment is an artificial aging treatment to eliminate residual stress. After the heat treatment, the blade still has a residual stress between −20 MPa and −80 MPa, and the heat treatment process should also be optimized. Although there are individual singular residual stress values of the blades after vibratory finishing and shot peening, they are negligible due to the small number.

The surface residual stress in the blade is further analyzed, and the average value and standard deviation of the surface residual stress of each process after blade machining can be obtained by calculation, as shown in Table 4. With the processing of blades from milling, polishing, heat treatment, vibratory finishing to shot peening, the average surface residual stress has also evolved from −305.87 MPa, −236.45 MPa, −46.46 MPa, −405.78 MPa, to −704.89 MPa, respectively. Standard deviation is analyzed by comparison. It is found that the standard deviation of residual stress after milling and polishing is greater than the measurement error of residual stress (±30 MPa), and the standard deviation of residual stress after heat treatment, vibration finishing and shot peening is less than or close to the measurement error of residual stress. The residual stress profile is determined by a variety of factors. The residual stress after milling is determined by the structure of the workpiece and the parameters of the milling process, and most of the residual stress profile is not very uniform. However the residual stress after polishing process is generally more uniform [12], and the standard deviation of the residual stress after polishing in this paper is greater than the measurement error, indicating that the processing stability is poor. It is suggested that the subsequent polishing process optimization should be combined with the blade structure to make the residual stress distribution as uniform as possible.

3.3 Residual stress distribution based on Rational Taylor surface function

According to the results of measured surface residual stress after blade processing, the two-dimensional distribution of blade residual stress is numerically fitted based on surface coordinates x, y, and the two-dimensional distribution formula of residual stress was obtained. In order to improve the fitting accuracy, the surface coordinates and surface residual stres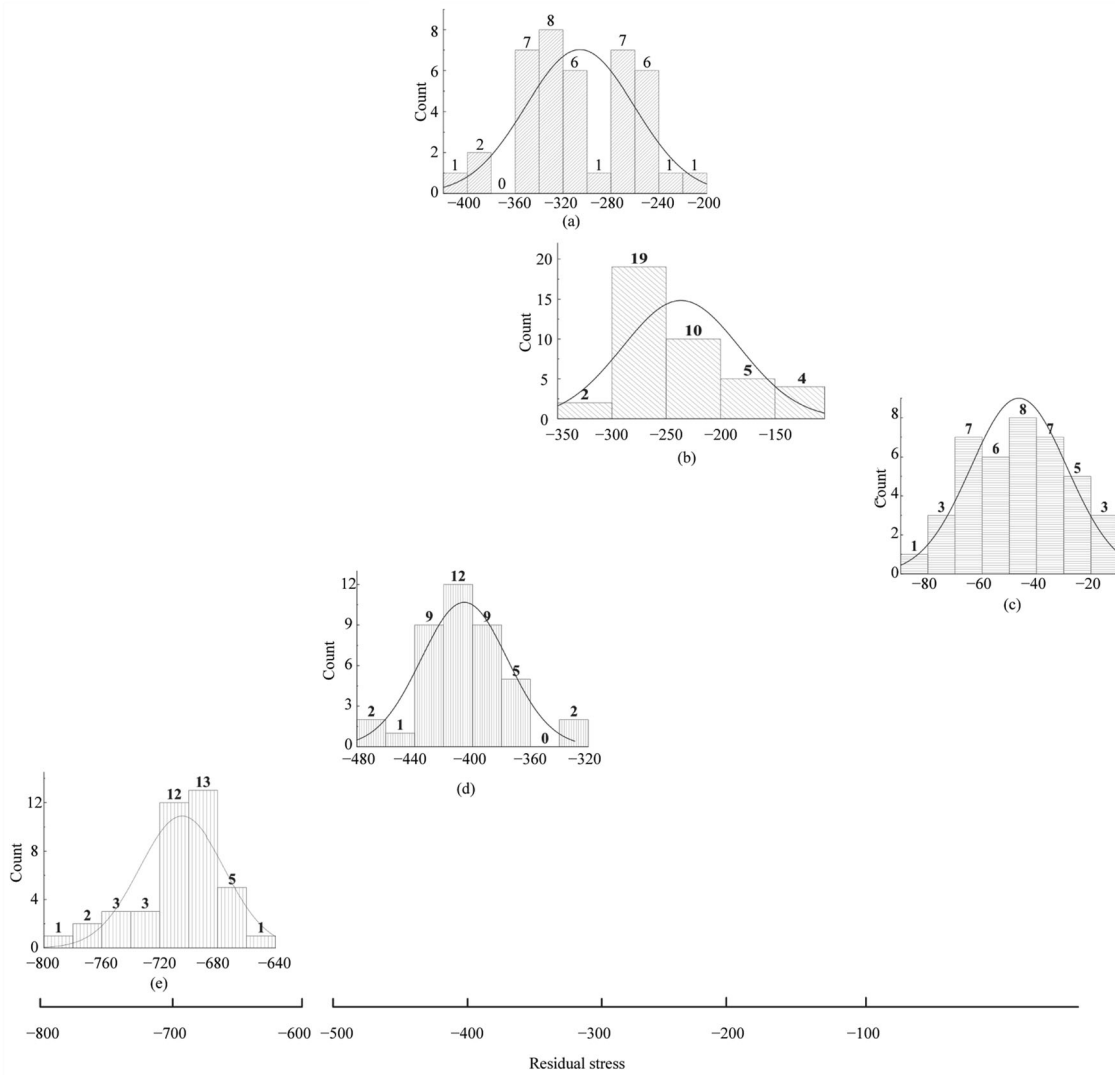s of blade need to be processed by mean-subtraction before fitting to avoid the influence of abnormal values and extreme values. The formula of mean-subtraction is shown as follows

Table 2 Extreme values of compressive residual stress on blade back

Process	Maximum		Minimum	
	Position	Value/MPa	Position	Value/MPa
Milling	Ridge area of blade root	− 405.30	Exhaust side area of blade middle	− 250.39
Polishing	Ridge area of blade tip	− 274.91	Intake side area of blade middle	− 108.30
Heat treatment	Exhaust side area of blade middle	− 85.22	Intake side area of blade tip	33.10
Vibratory finishing	Exhaust side area of blade tip	− 472.71	Exhaust side area of blade root	− 331.77
Shot peening	Ridge area of blade middle	− 784.77	Intake side area of blade root	− 658.58

Table 3 Extreme values of compressive residual stress on blade basin

Process	Maximum		Minimum	
	Position	Value/MPa	Position	Value/MPa
Milling	Exhaust side area of blade root	− 380.56	Intake side area of blade middle	− 210.56
Polishing	Intake side area of blade tip	− 321.28	Ridge area of blade middle	− 211.89
Heat treatment	Intake side area of blade middle	− 67.88	Exhaust side area of blade root	− 3.17
Vibratory finishing	Intake side area of blade middle	− 459.64	Exhaust side area of blade tip	− 369.24
Shot peening	Exhaust side area of blade middle	− 760.65	Intake side area of blade middle	− 661.51

Fig. 4 Statistical distributions of residual stress in the blade surface **a** milling, **b** polishing, **c** heat treatment, **d** vibratory finishing, **e** shot peening

$$\begin{cases} x' = x - \mu, \\ y' = y - \mu, \\ \sigma' = \sigma - \mu, \end{cases} \quad (4)$$

where x', y' and σ' are the values of mean-subtraction; x, y and σ are the actual measured values; μ is the average value of the actual data.

$$\sigma = \frac{z_0 + A_{01}x + B_{01}y + B_{02}y^2 + C_{02}xy}{1 + A_1x + B_1y + A_2x^2 + B_2y^2 + C_2xy}. \quad (5)$$

The Rational Taylor surface function shown in Eq. (5) is used to fit the surface residual stress distribution of the blade. The surface coordinates and surface residual stress

of blade are processed by mean-subtraction according to Eq. (4) before fitting. The coordinates and the residual stress of each process based on Eq. (4) are shown in Table 5.

The parameters of the fitting empirical formula based on Eq. (5) are shown in Table 6. R^2 is the goodness of fit of the empirical formula, and the goodness of fit is extremely close to 1, indicating that the accuracy of the fitting is high.

Combining Eqs. (4) and (5), the fitting formula for the actual surface residual stress distribution of the blade based on the surface position x and y (as shown in Fig. 2) can be obtained, and $-75 \leq x \leq 75, 200 \leq y \leq 600$.

4 Analysis of subsurface residual stress of the blade

4.1 Distribution of subsurface residual stress

The distributions of the residual stress along the depth based on the measurement data of the blade back and blade basin are shown in Fig. 5. The distribution trend of the residual stress in the blade back and the blade basin along the depth direction is generally consistent, but the residual stress value at each point of the same depth is different. The compressive residual stress in the surface of the blade after milling is about −300 MPa. With the increase of the depth, the compressive residual stress gradually decreases, and finally reduces to about 0 MPa at a depth of 50–60 μm. This is the residual stress value of the milled blade base, and the depth of the residual stress field is about 50 μm. The compressive residual stress in the surface of the blade after polishing is about −300 MPa. With the increase of the depth, the compressive residual stress gradually decreases and finally reduces to about 0 MPa at a depth of 30–40 μm, and the depth of the residual stress field is about 40 μm. The compressive residual stress in the surface of the blade after heat treatment is about −50 MPa. With the increase of the depth, the compressive residual stress gradually decreases and finally reduces to about 0 MPa at a depth of 20 μm, and the depth of the residual stress field is about 20 μm. The compressive residual stress in the surface of the blade after vibratory finishing is about −400 MPa. With the increase of the depth, the compressive residual stress gradually decreases and finally reduces to about 0 MPa at a depth of 50 μm, and the depth of the residual stress field is about 50 μm. The compressive residual stress in the surface of the blade after shot peening is about −700 MPa, and the compressive residual stress gradually increases with the increase of the depth, which reaches the maximum value at a depth of 30 μm. Compared with the value of surface residual stress, each area increases by several tens in varying degrees. Then the compressive residual stress gradually decreases with increasing depth and finally decreases to about 0 MPa at a depth of 150 μm, and the depth of the residual stress field is about 150 μm.

4.2 Residual stress distribution based on cosine decay function

According to the measured residual stress after blade machining, the depth distribution of residual stress is modeled based on the depth h, and the depth distribution formula of residual stress is obtained. To improve the fitting accuracy, the depth h and subsurface residual stress need to be processed by min-max normalization before fitting to avoid the influence of abnormal values and extreme values. The formula is shown as follows

$$b'' = (b - b_{\min})/(b_{\max} - b_{\min}), \tag{6}$$

where b'' is the value of min-max normalization; b is the actual measured value; $b_{\max}$ is the maximum value of the measurement data; $b_{\min}$ is the minimum value of the measurement data.

$$\sigma(h) = A e^{\lambda h} \cos(\omega h + \theta) + \sigma_0. \tag{7}$$

The cosine decay function shown in Eq. (7) is used to fit the surface residual stress distribution along the depth. The depth value and residual stress value are processed by min-max normalization according to Eq. (6). The parameters of each process based on Eq. (6) are shown in Table 7.

The parameters of the fitting empirical formula based on Eq. (7) are shown in Table 8. R^2 in the table is the goodness of fit of the empirical formula, and the goodness of fit is extremely close to 1, indicating that the accuracy of the fitting is high.

Combining Eqs. (6) and (7), the fitting formula of the actual subsurface residual stress distribution along the depth of the blade based on the depth position h can be obtained.

5 Three-dimensional modeling and reconstructive change of residual stress

5.1 Three-dimensional modeling of residual stress

According to Eqs. (5) and (7), the parametric modeling based on the space coordinates x, y, h of the blade is performed to obtain the three-dimensional distribution model

Table 4 Average value, and standard deviation of surface residual stress of blade

Process	Average value/MPa	Standard deviation/MPa
Milling	− 305.87	45.42
Polishing	− 236.45	53.90
Heat treatment	− 46.46	17.73
Vibratory finishing	− 405.78	29.89
Shot peening	− 704.89	29.25

Table 5 Parameters of the mean-subtraction formula for each process

	Milling	Polishing	Heat treatment	Vibratory finishing	Shot peening
x_μ/mm	− 4.87	− 3.62	− 2	− 2	− 2
y_μ/mm	379.14	374.12	371.62	371.62	371.62
σ_μ/MPa	− 306.11	− 236.45	− 46.46	− 410.12	− 704.89

of the residual stress for each process, as shown in Eqs. (8)–(12).

$$
\begin{cases}
\sigma_{\mathrm{M}} = 469.20(\exp(-2.65h'')\cos(-3.99h'' + 4.08) + 0.51) + \sigma_{M-x,y'}, \\
\sigma_{M-x,y} = \dfrac{-0.48 - 10.38x' - 2.37y' - 9.74\mathrm{e}^{-2}y'^2 - 3.47\mathrm{e}^{-2}x'y'}{1 - 6.97x' - 0.82y' - 0.22x'^2 + 3.63\mathrm{e}^{-2}y'^2 - 0.12x'y'} - 306.11, \\
h'' = h/60, \\
x' = x + 4.87, \\
y' = y - 379.14, \\
-75 \le x \le 75, \\
200 \le y \le 600, \\
0 \le h \le 60.
\end{cases}
\tag{8}
$$

$$
\begin{cases}
\sigma_{\mathrm{P}} = 2097.27(\exp(-0.05h'')\cos(-0.44h'' + 0.59) - 0.85) + \sigma_{P-x,y'}, \\
\sigma_{P-x,y} = \dfrac{14.57 + 2.93\mathrm{e}^{-2}x' + 0.60y' + 3.31\mathrm{e}^{-3}y'^2 + 3.67\mathrm{e}^{-5}x'y'}{1 + 0.27x' - 0.23y' + 3.79\mathrm{e}^{-2}x'^2 - 2.68\mathrm{e}^{-3}y'^2 - 4.91\mathrm{e}^{-3}x'y'} - 236.45, \\
h'' = h/40, \\
x' = x + 3.62, \\
y' = y - 374.12, \\
-75 \le x \le 75, \\
200 \le y \le 600, \\
0 \le h \le 40.
\end{cases}
\tag{9}
$$

$$
\begin{cases}
\sigma_{\mathrm{Ht}} = -155.89(\exp(-0.66h'')\cos(-2.64\mathrm{e}^{-4}h'' + 1.02) - 0.46) + \sigma_{Ht-x,y'}, \\
\sigma_{Ht-x,y} = \dfrac{-0.62 + 3.9\mathrm{e}^{-2}x' + 2.14\mathrm{e}^{-2}y' + 1.83\mathrm{e}^{-4}y'^2 - 4.24\mathrm{e}^{-5}x'y'}{1 - 4.54\mathrm{e}^{-3}x' + 1.28\mathrm{e}^{-2}y' - 3.35\mathrm{e}^{-4}x'^2 - 6.24\mathrm{e}^{-6}y'^2 + 2.23\mathrm{e}^{-4}x'y'} - 46.46, \\
h'' = h/20, \\
x' = x + 2, \\
y' = y - 371.62, \\
-75 \le x \le 75, \\
200 \le y \le 600, \\
0 \le h \le 20.
\end{cases}
\tag{10}
$$

$$
\begin{cases}
\sigma_{\mathrm{Vf}} = 1131.75(\exp(-2.56h'')\cos(-0.95h'' + 4.28) + 0.45) + \sigma_{Vf-x,y'}, \\
\sigma_{Vf-x,y} = \dfrac{9248.72 + 161.62x' + 94.42y' + 0.25y'^2 + 0.99x'y'}{1 - 55.84x' - 5.45y' - 1.06x'^2 - 5.34\mathrm{e}^{-2}y'^2 - 0.90x'y'} - 410.12, \\
h'' = h/50, \\
x' = x + 2, \\
y' = y - 371.62, \\
-75 \le x \le 75, \\
200 \le y \le 600, \\
0 \le h \le 50.
\end{cases}
\tag{11}
$$

Table 6 Parameters of the Rational Taylor surface function for each process

	Milling	Polishing	Heat treatment	Vibratory finishing	Shot peening
z_0	− 0.479	14.571	− 0.624	9248.727	46.799
A_{01}	− 10.382	0.029	0.004	161.619	− 1.885
B_{01}	− 2.374	0.603	0.021	94.417	− 0.258
B_{01}	− 0.097	0.003	1.828×10^{-4}	0.249	0.001
B_{02}	− 0.034	3.667×10^{-5}	-4.245×10^{-5}	0.994	− 0.005
C_{02}	− 6.969	0.266	− 0.005	− 55.838	− 0.426
A_1	− 0.220	0.0379	-3.350×10^{-4}	− 1.055	0.014
A_2	− 0.819	− 0.229	0.013	− 5.452	0.036
B_2	0.036	− 0.003	-6.242×10^{-6}	− 0.053	-3.843×10^{-4}
C_2	− 0.121	− 0.005	2.228×10^{-4}	− 0.902	0.003
R^2	0.970	0.969	0.992	0.986	0.978

$$\begin{cases} \sigma_{\mathrm{Sp}} = 177.06(\exp(1.17h'') \cos(-3.83h'' + 3.36) + 0.99) + \sigma_{Sp-x,y'}, \\ \sigma_{Sp-x,y} = \dfrac{46.79 - 1.88x' - 0.26y' + 1.02\mathrm{e}^{-3}y'^2 - 5.46\mathrm{e}^{-3}x'y'}{1 - 0.43x' + 3.66\mathrm{e}^{-2}y' + 1.36\mathrm{e}^{-2}x'^2 - 3.84\mathrm{e}^{-4}y'^2 + 2.89\mathrm{e}^{-3}x'y'} - 704.89, \\ h'' = h/180, \\ x' = x + 2, \\ y' = y - 371.62, \\ -75 \leq x \leq 75, \\ 200 \leq y \leq 600, \\ 0 \leq h \leq 180. \end{cases} \quad (12)$$

In Eqs. (8)–(12), σ_{M}, σ_{P}, σ_{Ht}, σ_{Vf}, and σ_{Sp} respectively represent the three-dimensional residual stress of the blade after milling, polishing, heat treatment, vibration finishing, and shot peening. Taking the milling process as an example, the three-dimensional distribution of residual stress after milling is shown in Fig. 6. The residual stress on the surface varies from position to position. For each position on the surface, the trend along the depth is roughly the same. However, due to the difference in surface residual stress, the residual stress values at different positions at the same depth are also different.

To verify the validity of the residual stress prediction formula, three points were selected for each process, and their coordinates (expressed as (x, y, h)) were substituted into the formula to calculate the residual stress values and compare them with the measured values. Comparing the results as shown in Fig. 7, the calculation error of heat treatment residual stress is the smallest, which is less than the measurement error (± 30 MPa); the calculation errors of residual stress for milling, polishing, vibration finishing and shot blasting are 15.7%, 20.8%, 21.6% and 6.4%, respectively. The calculation errors are all less than 25%,

and the formulas have a high accuracy to characterize the residual stress distribution of each process.

5.2 Reconstructive change of residual stress

The reconstructive change of residual stress among multiple processes is shown in Fig. 8. It can be seen from Fig. 8 that the trend of the fitting curve of the residual stress distribution along the depth direction of each process is basically the same. The maximum residual stress is in the surface or subsurface, and then the compressive residual stress decreases with the depth increase until it decreases to about 0 MPa, but the residual stress value at the same depth has a certain degree of dispersion.
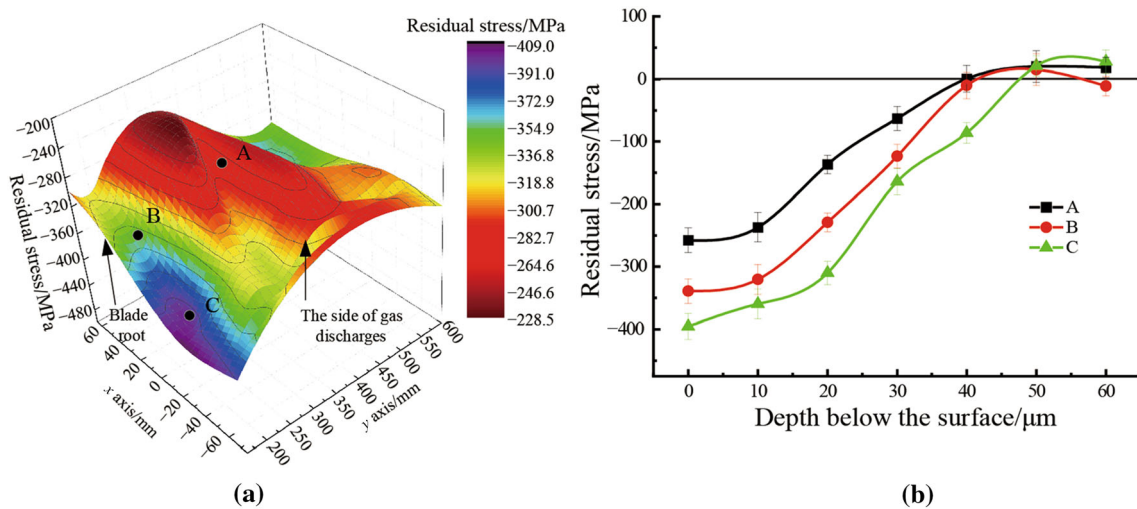
The evolution of the residual stress distribution of each process is comparatively analyzed in Fig. 8. It can be found that as the first process of blade machining, the surface residual stress after milling is about −300 MPa, and the depth of the residual stress field is 60 μm. Subsequently, due to the removal amount of 10–20 μm in the polishing process, the compressive residual stress in the surface is reduced to about −260 MPa, and the depth of the residual
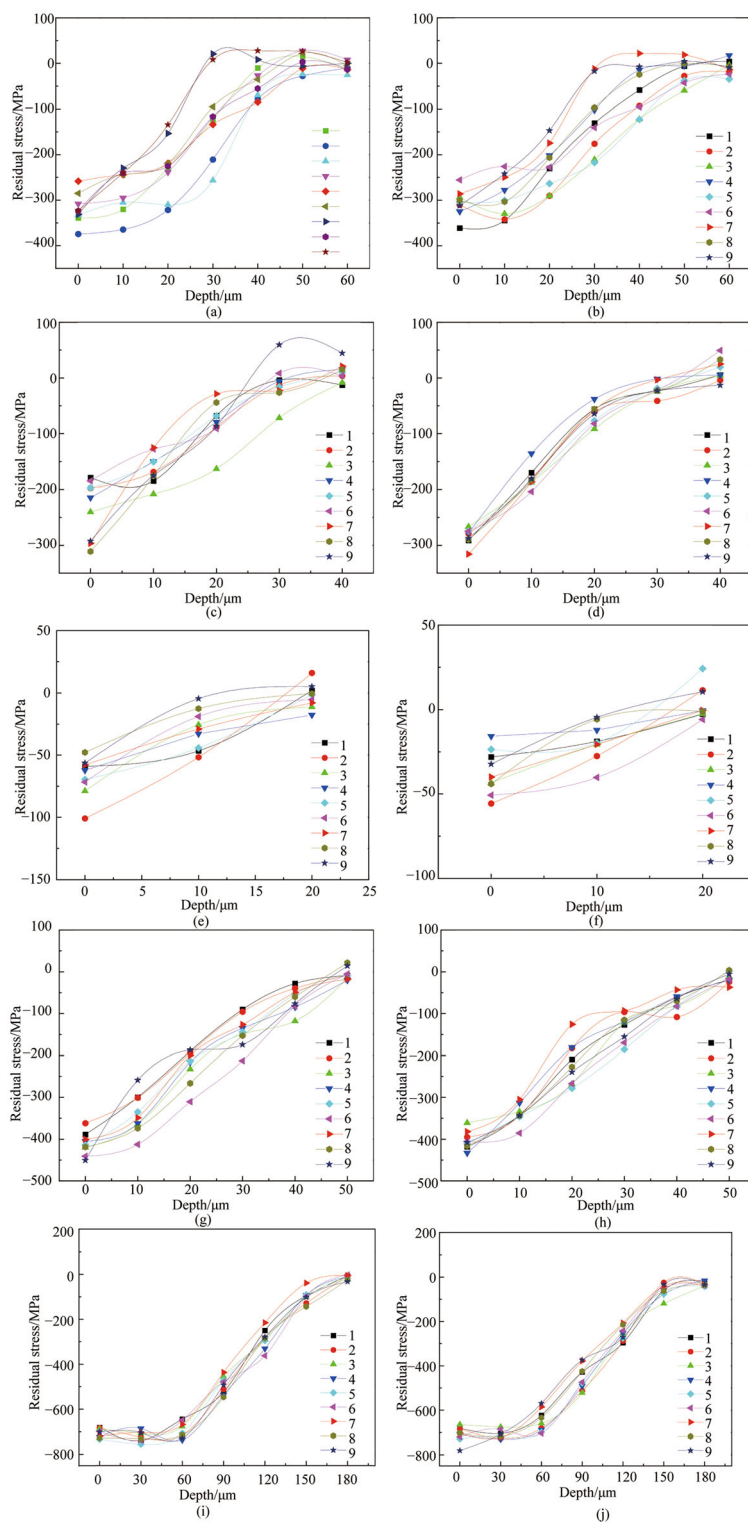
Fig. 5 Distributions of residual stress along depth **a** blade back of milled blade, **b** blade basin of the milled blade, **c** blade back of the blade after polishing, **d** blade basin of the blade after polishing, **e** blade back of the blade after heat treatment, **f** blade basin of the blade after heat treatment, **g** blade back of blade after vibratory finishing, **h** blade basin of the blade after vibratory finishing, **i** blade back of blade after shot peening, **j** blade basin of the blade after shot peening

stress field is also reduced to about 40 μm. After heat treatment for the purpose of stress removal, the

compressive residual stress in the surface is reduced to about −50 MPa, and the depth of the residual stress field is

Fig. 6 Three-dimensional distributions of the residual stress for the blade. take the milled blade as an example **a** distribution of surface residual stress, **b** distribution of subsurface residual stress

Table 7 Parameters of the min-max normalization formula for each process

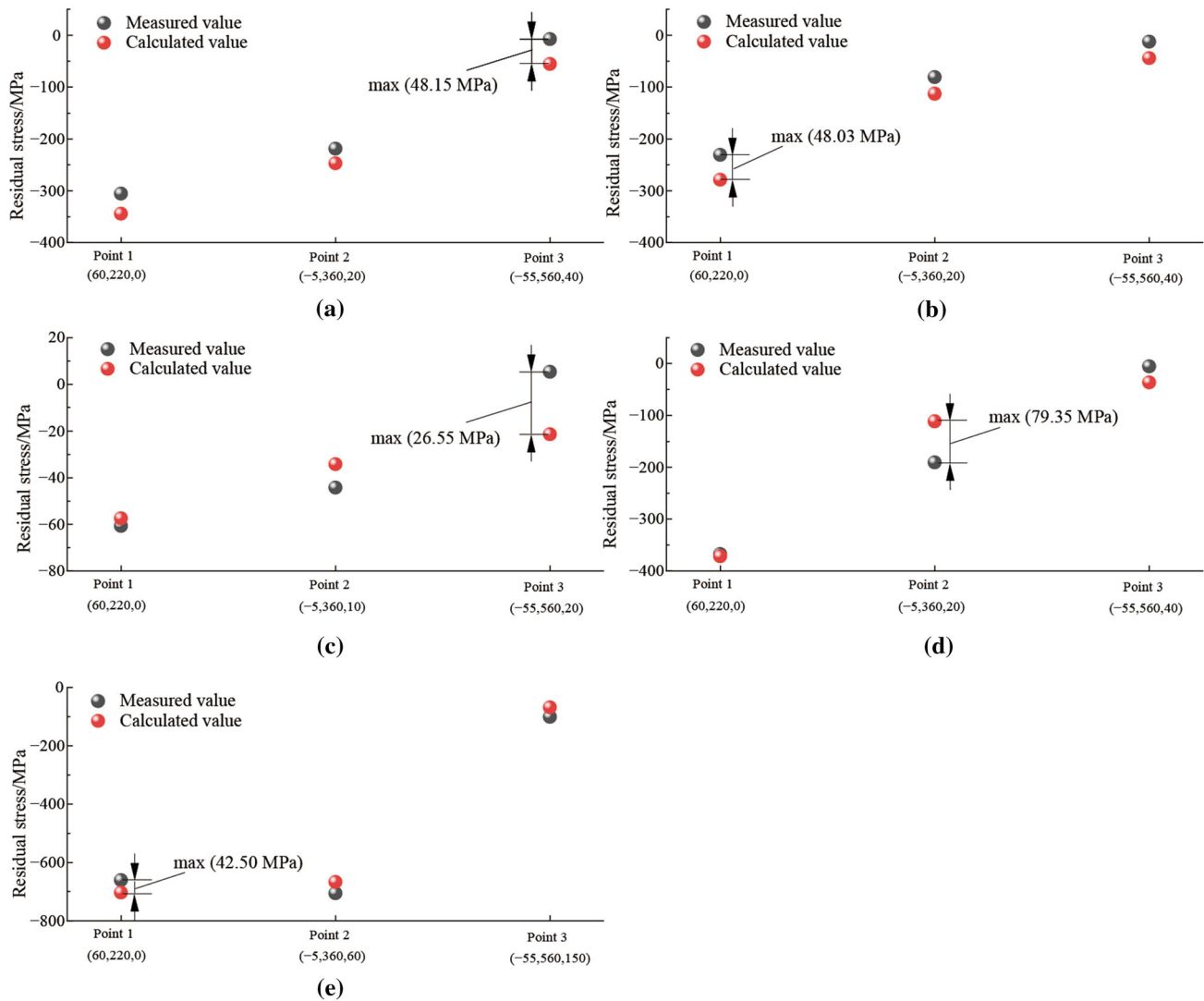|	Milling	Polishing	Heat treatment	Vibratory finishing	Shot peening
h_{max}/μm	60	40	20	50	180
h_{min}/μm	0	0	0	0	0
σ_{max}/MPa	0	0	0	0	0
σ_{min}/MPa	− 400	− 315	− 70	− 450	− 780

Table 8 Parameters of the cosine decay function for each process

	Milling	Polishing	Heat treatment	Vibratory finishing	Shot peening
A	1.173 15	6.658 45	− 2.226 90	2.515 29	0.226 64
λ	− 2.653 41	− 0.045 91	− 0.662 82	− 2.565 93	1.169 49
ω	− 3.997 96	− 0.438 44	− 0.000 26	− 0.949 76	− 3.832 08
θ	4.081 98	0.595 82	1.017 31	4.283 27	3.366 06
σ_0	0.829 18	− 5.402 80	1.364 68	1.122 51	0.321 19
R^2	0.974 28	0.983 33	0.989 09	0.937 99	0.995 99

also reduced to 10–20 μm. The heat treatment process is to eliminate the residual stress, but the blade in this study still has a certain amount of residual stress after heat treatment exists. It is recommended that the subsequent process optimization should be carried combined with the blade structure and make the residual stress relief after heat treatment more complete. The vibratory finishing process to improve the surface quality increases the compressive surface residual stress to about −420 MPa, and the depth of the residual stress field also increases to about 50 μm, similar to the milling process. The last manufacturing process of shot peening greatly improved fatigue strength. The surface residual stress increased to about −700 MPa,

and the depth of the residual stress field also increased to about 180 μm. Due to different processing purposes, the residual stress field introduced by each process is also different.

For further comparative analysis, on the surface, the residual stress is −300 MPa after milling, −250 MPa after polishing, −50 MPa after heat treatment, −400 MPa after vibration finishing, and −720 MPa after shot peening. At a depth of 20μm, −250 MPa for milling, −100 MPa for polishing, heat treatment is 0 MPa, −300 MPa for vibration finishing, and −720 MPa for shot peening. At a depth of 40 μm, milling is −50 MPa; polishing is 0 MPa; vibratory finishing is about −50 MPa; and shot peening is

Fig. 7 Measured and calculated values of residual stress **a** milling, **b** polishing, **c** heat treatment, **d** vibratory finishing, **e** shot peening

−700 MPa. The residual stresses of milling and vibratory finishing are 0 MPa at a depth of 60 μm and 50 μm, respectively. The compressive residual stresses on the surface of vibratory finishing are greater than those of milling, but the depth of the affected layer is smaller than that of milling. The residual stress is 0 MPa at 180 μm depth after shot peening.

Equations (8)–(12) describe the empirical formula of the residual stress distribution of each process. The goodness of fit is extremely close to 1, and the fitting accuracy is high, showing that the residual stress distribution law is highly consistent. The residual stress distribution of each processing technology of the blade is taken as the target, and the surface and subsurface residual stress of the blade is analyzed by statistics and fitting. It can be intuitively seen the distribution of residual stress in each process and the evolution between them.

Large fan blades are prone to deformation problems during milling, polishing, heat treatment, vibratory finishing and shot peening, and fatigue problems after shot peening should also be considered. The residual stress distribution and evolution of multiple processes of large fan blades in this study can guide the solution of blade machining deformation [41] and fatigue aging problems from the perspective of residual stress. It has a valuable reference for the subsequent research on the residual stress of various processes of large fan blades.

6 Conclusions

In this paper, the large fan blade of titanium alloy is taken as the research object; the whole process of the blade from the blank to the finished product is processed; and a series
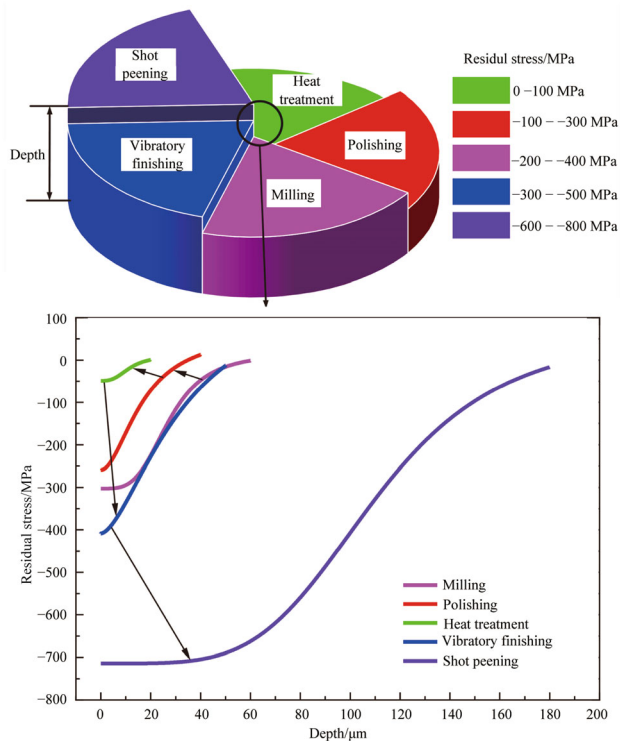
Fig. 8 Evolution of residual stress distribution along the depth direction of each machining process

of studies are carried out on the residual stress after each process. The main research results of this paper mainly include the following aspects.

(i) The surface and subsurface residual stresses of the blade after multiple processes (milling, polishing, heat treatment, vibratory finishing, shot peening) were measured. Combined with the position of the blade profile, the surface residual stress distribution of each process is analyzed, and the extreme value of the residual stress of each process is summarized.

(ii) According to the residual stress data of measurement points for each process, the distribution of residual stress is analyzed, and the Rational Taylor surface function and cosine decay function are used to fit the characteristic function of the residual stress distribution. Some well-fitting empirical formulas are obtained. The distributions of the residual stress in each process are quite different due to different processes.

(iii) The analysis in which the evolution of the surface and subsurface residual stress of the blade's multi-process provides an idea for the subsequent research on the residual stress of blade after manufacturing and has a high guiding significance for the optimization of each process.

References

1. Yao C, Zhang J, Cui M et al (2020) Machining deformation prediction of large fan blades based on loading uneven residual stress. Int J Adv Manuf Technol 107(9/10):4345–4356
2. Guo M, Jiang X, Ye Y et al (2019) Investigation of redistribution mechanism of residual stress during multi-process milling of thin-walled parts. Int J Adv Manuf Technol 103(1/4):1459–1466
3. El-Khabeery MM, Fattouh M (1989) Residual stress distribution caused by milling. Int J Mach Tools Manuf 29(3):391–401
4. Wang J, Zhang D, Wu B et al (2017) Residual stresses analysis in ball end milling of nickel-based superalloy Inconel 718. Mater Res 20(6):1681–1689
5. Ji C, Sun S, Lin B et al (2018) Effect of cutting parameters on the residual stress distribution generated by pocket milling of 2219 aluminum alloy. Adv Mech Eng 10(12). https://doi.org/10.1177/1687814018813055
6. Kong X, Ding Z, Xu L et al (2019) Effects of milling parameters on distribution of residual stress during the milling of curved thin-walled parts. EPJ Web Conf 224:5009. https://doi.org/10.1051/epjconf/201922405009
7. Fuh KH, Wu CF (1995) A residual-stress model for the milling of aluminum alloy (2014–T6). J Mater Process Technol 51(1/4):87–105
8. Peng FY, Dong Q, Yan R et al (2016) Analytical modeling and experimental validation of residual stress in micro-end-milling. Int J Adv Manuf Technol 87(9/12):3411–3424
9. Yang D, Liu Z, Ren X et al (2016) Hybrid modeling with finite element and statistical methods for residual stress prediction in peripheral milling of titanium alloy Ti-6Al-4V. Int J Mech Sci 108/109:29–38
10. Wang J, Zhang D, Wu B et al (2017) Numerical and empirical modelling of machining-induced residual stresses in ball end milling of Inconel 718. Procedia CIRP 58:7–12
11. Zhou R, Yang W (2019) Correction to: analytical modeling of residual stress in helical end milling of nickel-aluminum bronze. Int J Adv Manuf Technol 100(1/4):1011
12. Qi H, Xie Z, Hong T et al (2017) CFD modelling of a novel hydrodynamic suspension polishing process for ultra-smooth surface with low residual stress. Powder Technol 317:320–328
13. Lin X, Wu D, Shan X et al (2018) Flexible CNC polishing process and surface integrity of blades. J Mech Sci Technol 32(6):2735–2746
14. Wu D, Wang H, Zhang K et al (2019) Research on flexible adaptive CNC polishing process and residual stress of blisk blade. Int J Adv Manuf Technol 103(5/8):2495–2513
15. Xiao G, Huang Y, Yin J (2017) An integrated polishing method for compressor blade surfaces. Int J Adv Manuf Technol 88(5/8):1723–1733
16. Yuan F, Liu C, Gu H et al (2019) Effects of mechanical polishing treatments on high cycle fatigue behavior of Ti-6Al-2Sn-4Zr-2Mo alloy. Int J Fatigue 121:55–62
17. Minguela J, Slawik S, Mücklich F et al (2020) Evolution of microstructure and residual stresses in gradually ground/polished 3Y-TZP. J Eur Ceram Soc 40(4):1582–1591

18. Sridhar BR, Devananda G, Ramachandra K et al (2003) Effect of machining parameters and heat treatment on the residual stress distribution in titanium alloy IMI-834. J Mater Process Technol 139(1/3):628–634

19. Bensely A, Venkatesh S, Mohan Lal D et al (2008) Effect of cryogenic treatment on distribution of residual stress in case carburized En 353 steel. Mater Sci Eng A 479(1/2):229–235

20. Paddea S, Francis JA, Paradowska AM et al (2012) Residual stress distributions in a P91 steel-pipe girth weld before and after post weld heat treatment. Mater Sci Eng A 534:663–672

21. Dong P, Song S, Zhang J (2014) Analysis of residual stress relief mechanisms in post-weld heat treatment. Int J Press Vessels Pip 122:6–14

22. Araghchi M, Mansouri H, Vafaei R et al (2017) A novel cryogenic treatment for reduction of residual stresses in 2024 aluminum alloy. Mater Sci Eng A 689:48–52

23. Zhang Z, Ge P, Zhao GZ (2017) Numerical studies of post weld heat treatment on residual stresses in welded impeller. Int J Press Vessels Pip 153:1–14

24. Bai Q, Feng H, Si LK et al (2019) A novel stress relaxation modeling for predicting the change of residual stress during annealing heat treatment. Metall Mater Trans A 50(12):5750–5759

25. Fu Y, Gao H, Wang X et al (2017) Machining the integral impeller and blisk of aero-engines: a review of surface finishing and strengthening technologies. Chin J Mech Eng 30(3):528–543

26. Kacaras A, Gibmeier J, Zanger F et al (2018) Influence of rotational speed on surface states after stream finishing. Procedia CIRP 71:221–226

27. Luo S, Zhou L, Nie X et al (2019) The compound process of laser shock peening and vibratory finishing and its effect on fatigue strength of Ti-3.5Mo-6.5Al-1.5Zr-0.25Si titanium alloy. J Alloy Compd 783:828–835

28. Wong BJ, Majumdar K, Ahluwalia K et al (2019) Effects of high frequency vibratory finishing of aerospace components. J Mech Sci Technol 33(4):1809–1815

29. Zanger F, Kacaras A, Neuenfeldt P et al (2019) Optimization of the stream finishing process for mechanical surface treatment by numerical and experimental process analysis. CIRP Ann 68(1):373–376

30. Kim T, Lee JH, Lee H et al (2010) An area-average approach to peening residual stress under multi-impacts using a three-dimensional symmetry-cell finite element model with plastic shots. Mater Des 31(1):50–59

31. Ghasemi A, Hassani-Gangaraj SM, Mahmoudi AH et al (2016) Shot peening coverage effect on residual stress profile by FE random impact analysis. Surf Eng 32(11):861–870

32. Mahmoudi AH, Ghasemi A, Farrahi GH et al (2016) A comprehensive experimental and numerical study on redistribution of residual stresses by shot peening. Mater Des 90:478–487

33. Zhan K, Jiang CH, Ji V (2013) Uniformity of residual stress distribution on the surface of S30432 austenitic stainless steel by different shot peening processes. Mater Lett 99:61–64

34. Sherafatnia K, Farrahi GH, Mahmoudi AH et al (2016) Experimental measurement and analytical determination of shot peening residual stresses considering friction and real unloading behavior. Mater Sci Eng A 657:309–321

35. Hayashi M, Okido S, Suzuki H (2020) Residual stress distribution in water jet peened type 304 stainless steel. Quantum Beam Sci 4(2):18. https://doi.org/10.3390/qubs4020018

36. Lai HH, Cheng HC, Lee CY et al (2020) Effect of shot peening time on δ/γ residual stress profiles of AISI 304 weld. J Mater Process Technol 284:116747. https://doi.org/10.1016/j.jmatprotec.2020.116747

37. Yao C, Wu D, Ma L et al (2016) Surface integrity evolution and fatigue evaluation after milling mode, shot-peening and polishing mode for TB6 titanium alloy. Appl Surf Sci 387:1257–1264

38. Tan L, Zhang D, Yao C et al (2017) Evolution and empirical modeling of compressive residual stress profile after milling, polishing and shot peening for TC17 alloy. J Manuf Process 26:155–165

39. Wu D, Zhang D, Yao C (2018) Effect of turning and surface polishing treatments on surface integrity and fatigue performance of nickel-based alloy GH4169. Metals 8(7):549. https://doi.org/10.3390/met8070549

40. Sridhar BR, Nafde WG, Padmanabhan KA (1992) Effect of shot peening on the residual stress distribution in two commercial titanium alloys. J Mater Sci 27(21):5783–5788

41. Zhang J, Yao C, Tan L et al (2021) Shot peening parameters optimization based on residual stress-induced deformation of large fan blades. Thin-Walled Struct 161(1):107467. https://doi.org/10.1016/j.tws.2021.107467

Ji-Yin Zhang received the M.S. degree in Aeronautical and Astronautical Manufacturing Engineering from Northwestern Polytechnical University in 2018. Now he is a Ph.D. student at Northwestern Polytechnical University. His research interest is residual stress and deformation of thin-walled blades after shot peening.

Chang-Feng Yao received the Ph.D. degree in Aeronautical and Astronautical Manufacturing Engineering from Northwestern Polytechnical University in 2006. Now he is a Professor at Northwestern Polytechnical University. His research interests include precision and anti-fatigue machining of key components of Aeroengine.

Min-Chao Cui received the Ph.D. degree in Mechanical Engineering from Xi'an Jiaotong University in 2019. Meanwhile, he also received the Ph.D. degree in Intelligent Structures and Mechanics Systems Engineering from Tokushima University. His research interests include laser intelligent diagnosis and advanced characterization technology of materials.

Yun-Qi Sun received the M.S. degree in Aeronautical and Astronautical Manufacturing Engineering from Northwestern Polytechnical University in 2020. Now he is a Ph.D. student at Northwestern Polytechnical University. His research interest is surface integrity of vibratory finishing.

Liang Tan received the Ph.D. degree in Aeronautical and Astronautical Manufacturing Engineering from Northwestern Polytechnical University in 2018. Now he is an assistant research fellow at Northwestern Polytechnical University. His research interests include cutting mechanism and surface integrity control technology of Aeronautical materials.